Field performance of an all-semiconductor laser coherent Doppler lidar

Peter John Rodrigo* and Christian Pedersen

DTU Fotonik, Department of Photonics Engineering, Technical University of Denmark, 4000 Roskilde, Denmark
**Corresponding author: pejr@fotonik.dtu.dk*

Received March 14, 2012; revised April 13, 2012; accepted April 15, 2012;
posted April 16, 2012 (Doc. ID 164800); published June 7, 2012

We implement and test what, to our knowledge, is the first deployable coherent Doppler lidar (CDL) system based on a compact, inexpensive all-semiconductor laser (SL). To demonstrate the field performance of our SL-CDL remote sensor, we compare a 36 h time series of averaged radial wind speeds measured by our instrument at an 80 m distance to those simultaneously obtained from an industry-standard sonic anemometer (SA). An excellent degree of correlation ($R^2 = 0.994$ and slope $= 0.996$) is achieved from a linear regression analysis of the CDL versus SA wind speed data. The lidar system is capable of providing high data availability, ranging from 85% to 100% even under varying outdoor (temperature and humidity) conditions during the test period. We also show the use of our SL-CDL for monitoring the dependence of aerosol backscatter on relative humidity. This work points to the feasibility of a more general class of low-cost, portable remote sensors based on all-SL emitters for applications that require demanding laser stability and coherence.

OCIS codes: 010.3640, 140.5960.

Light detection and ranging (lidar) is a well-known laser technology for a variety of remote sensing applications. A common lidar variant is the so-called coherent Doppler lidar (CDL) [1], which collects a portion of laser backscatter from a moving target and coherently combines the received (frequency-shifted) signal with a reference beam incident on a sensitive photodetector. In this technique, the line-of-sight (LOS) or radial speed v_r of the target is deduced from the Doppler spectrum via frequency analysis of the photodetector beat signal according to a simple relation given by $v_r = \Delta f_c(\lambda/2)$, where λ is the laser wavelength and Δf_c is the centroid frequency of the Doppler spectral peak. CDL systems are able to interrogate not only hard targets but also diffuse targets, such as aerosol in the atmosphere. Furthermore, scalar CDL measurements can be extended to resolve velocity vectors by scanning the LOS axis [2] or intersecting several lidar beams [3].

The ability of CDL systems to obtain spatially resolved measurements of atmospheric wind velocity from remote locations has been applied to a growing number of applications such as characterization of wind farm [4], determination of wind turbine power curves [5], measurement of tropospheric wind profiles [6], air turbulence [3], aircraft wake vortices [7], and true airspeed [2]. Aside from the emerging demand attributed to the above applications, the departure of lidar developers from CO_2 laser based systems and their adoption of eye-safe narrow-linewidth fiber lasers and fiber amplifiers, originally developed for the telecom industry, have recently resulted in a notable increase in the availability of commercial lidars for atmospheric sensing. Nevertheless, these current lidar products remain relatively bulky and expensive, and have thus been primarily limited as scientific instruments. To address the need for a more industrial lidar solution, we have developed a compact and low-cost CDL system based on a novel semiconductor laser (SL) source: a 1550 nm monolithic-integrated master oscillator power amplifier (MOPA) SL [8,9]. In [9], we demonstrated a tabletop SL-CDL as a proof of principle. We emphasize that the MOPA-SL we employ is an "all"-semiconductor emitter. It must be differentiated from the MOPA source utilizing a low-power SL in tandem with a rare-earth-doped fiber amplifier, which causes spurious reflections or unwanted excess noise in a CDL system [10].

In this Letter, we report on the implementation and state-of-the-art performance of an enhanced SL-CDL that can be deployed in the field for extended outdoor testing. Our deployable SL-CDL is schematically shown in Fig. 1. It consists of two parts: (i) a control module wherein the laser, detector, and other sensitive electronic components are situated and (ii) a transceiver module with 3 in. exit/entrance aperture containing only passive optical components, which makes it robust in lightning-prone areas. In this rugged SL-CDL, the laser is pigtailed to a

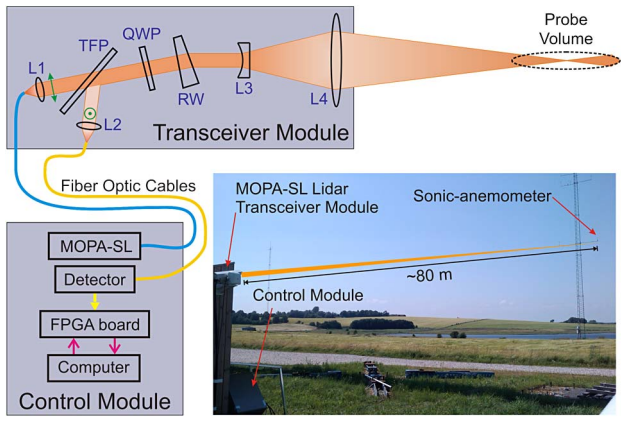

Fig. 1. (Color online) Schematic of a deployable SL-based homodyne cw lidar consisting of transceiver (15 cm × 15 cm × 45 cm) and control (50 cm × 30 cm × 75 cm) modules linked by two fiber optic cables. The "all-optical" transceiver is composed of collimating lens L1, thin-film polarizer (TFP), $\lambda/4$ wave plate (QWP), reference wedge (RW) for generating a local oscillator beam, telescope lenses L3 and L4, and coupling lens L2. All sensitive electronics are part of the control module. The inset shows a photo of the field test to compare the performance of our lidar wind sensor against a three-dimensional sonic anemometer (F2901 Metek, Germany).

polarization-maintaining fiber, which enables fiber optic delivery (5 m cable) of a stable TEM_{00} output beam with ~0.5 W cw power to the transceiver. Aside from the additional ruggedness, the new fiber-coupled SL-CDL system is easier to align and optimize compared to our previous free-space optics implementation [9]. In essence, the spatial filtering of the SL emission is instantly carried out by the first fiber coupling rather than by a careful selection of an appropriately sized aperture in the detector plane. Note that the beam emitted by a MOPA-SL chip is structured with a characteristic M^2~1.5 [9]. From the transceiver, the interfering reference beam and received signal are outcoupled to another single-mode optical fiber cable linked to the detector inside the control module. We employ an advanced FPGA-based data processor and algorithm previously developed (described in more detail in [9]) for analyzing the 50 MHz sampled detector signal. This enables us to produce and average raw Doppler spectra (with characteristic wind signal full width half maximum of ~1 to 2 MHz [9]) in real-time and obtain, at a user-defined update rate, reliable LOS speed estimates with maximum speed of ~19 ms^{-1} and bin resolution bin resolution = 0.04 ms^{-1}. We emphasize that the use of a fast processor is vital in the spectral averaging procedure, particularly in the use of CDL as a wind sensor where the aerosol in the probe volume has a characteristically low backscatter coefficient (in the order of 10^{-6} to 10^{-5} $m^{-1}\,sr^{-1}$). Phase-to-intensity noise [10,11] has been sufficiently reduced in our CDL design to ensure shot-noise-limited operation. As in typical CDL systems, spectral (or incoherent) averaging allows us to mitigate signal fading due to speckle effects. Moreover, the watt-level power and narrow linewidth (order of hundred kHz) of the MOPA-SL [9] are also beneficial to the performance of our SL-CDL as a wind sensor, which we investigate here in a field test.

The inset of Fig. 1 shows a photograph of the field test conducted at the Risø-DTU test site in Denmark. The lidar transmit beam is focused at 80 m radial distance adjacent to a reference sonic anemometer (SA) mounted at 18 m elevation on a meteorological mast. The SA supplies data at a rate of 32 Hz for all three orthogonal components of the local wind field, which allows us to extract SA-based data of wind speed components along the lidar LOS axis for side-by-side comparison with the lidar data. Radial speed estimates by the lidar were also gathered at 32 Hz. But to circumvent the filtering effect due to spatial volume averaging by the lidar [12] and relax the precise synchronization of the two data sets, we processed the measurements of both sensors into 10 min averages. In Fig. 2a, the data sets of the lidar and SA based on 10 min averages are plotted, together with their difference (Lidar–Sonic), which uses the right-hand y-axis scale. The mean and standard deviations of the difference plot are –0.06 and 0.18 ms^{-1}, respectively. The excellent agreement of the two sensors is presented in an alternative way in a regression analysis shown in Fig. 2b, where least squares fit of the lidar-versus-SA data scatter to either $y = mx$ or $y = mx + b$ resulted in R^2 and m values close to unity. Based on these quantitative figures of merit, the performance of our SL-CDL is found to be at par with that of commercial fiber laser amplifier-based cw lidars [13]. A careful look at the data

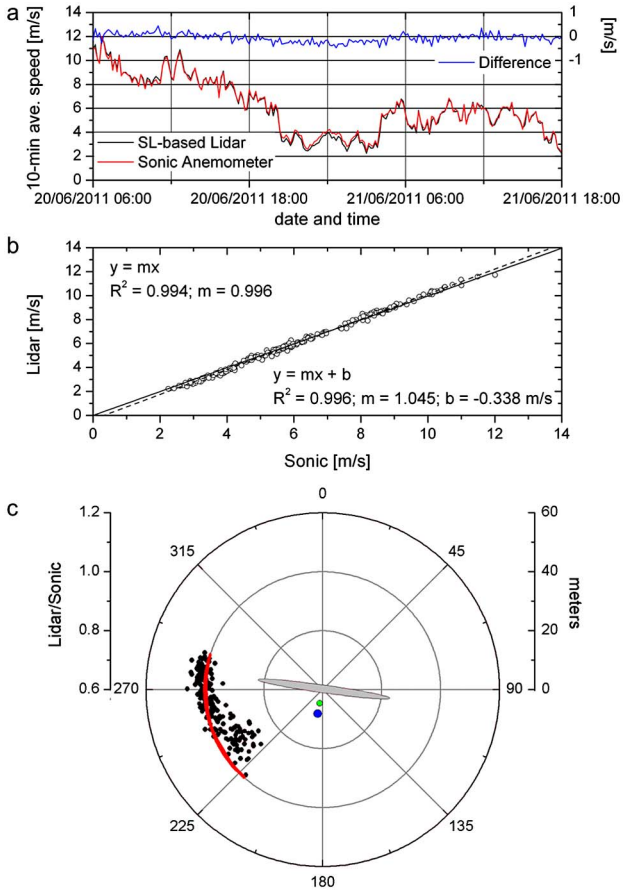

Fig. 2. (Color online) 36 h radial wind speed data. a. 10 min averages and the difference (right axis). b. Linear regression of the data. c. Polar plot of the lidar/sonic ratio (black points) as a function of horizontal wind direction. The red arc denotes the lidar/sonic ratio equal to 1. The gray ellipse depicts the lidar beam extent to be approximately twice the Rayleigh length (quadratically dependent on range) and its azimuthal orientation. Green (small) and blue (large) dots mark the positions of the SA and the mast relative to the probe beam, respectively.

explains the negative bias, i.e., b = –0.34 ms^{-1} (and m slightly greater than unity). We note that this is primarily due to a 6 h long middle portion of the time series, when the lidar evidently underestimated the wind speed relative to the SA data. We observed, as illustrated in Fig. 2c, that the wind directions associated with the said period are those that give rise to mast flow distortion within the probe volume (characterized by focused beam waist and Rayleigh length). Such mast wake effect has been observed in previous lidar tests [14].

For our target application in turbine yaw and blade pitch control, the lidar has an advantage in terms of its ability to actually measure the undisturbed wind in front of the turbine. Most control systems currently rely on conventional instrumentation mounted on top of the turbine nacelle, where considerable turbulence created by the rotor blades inevitably results in inaccurate estimates.

The manner in which the current lidar outputs a 10 min average wind speed is as follows: for every 10 min interval, each 32 Hz average spectrum (i.e., amplitude values corresponding to 511 frequency bins) is

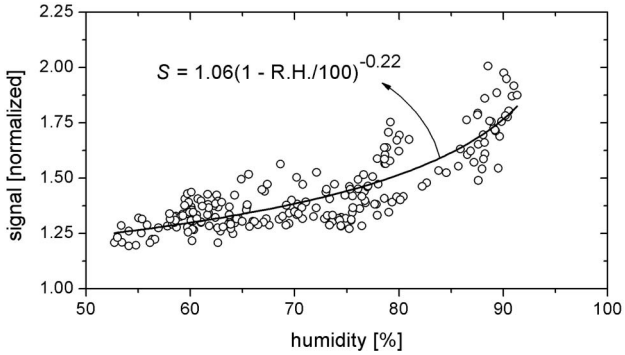

Fig. 3. Dependence of the signal (normalized to shot noise) on RH during the 36 h field test. From RH of 53% to 91%, the signal strength, relative to shot noise, increased by a factor of ~4.

first sent through a screening algorithm that categorizes the spectrum as either "reliable" or "rejected." A spectrum is rejected when either (A) its maximum amplitude is below a set amplitude threshold (to distinguish the signal from noise floor fluctuations), or (B) the measured centroid frequency is below a chosen cutoff frequency of ~2 MHz (to avoid both sign ambiguity issues and detection of residual low-frequency noise that affect wind speed averaging). It is only the reliable spectra that get further processed for Δf_c estimation, which produced the lidar $\langle v_r \rangle$ data in Fig. 2. During the field test, we were able to track the percentage of reliable spectrum for each 10 min average (i.e., data availability). We find that all averaged points have corresponding data availability exceeding 85% (average $= 97.8 \pm 2.5\%$), which is indicative of the reliable stability of the laser and the lidar as a whole during the entire test period. Note that even for 10 min averaging, reduction in data availability increases the probability of mismatch between lidar and sonic measurements because a dynamic LOS wind speed variation may be improperly averaged. We also monitored the temperature and relative humidity (RH; measured using additional transducers) of the outside environment at the site where the field test was conducted.

For the 36 h test, the SL-CDL has operated with sufficient signal-to-noise ratio (SNR) despite the known effects of changing atmospheric conditions on SNR. This is elaborated in Fig 3, which shows a plot of the shot-noise-normalized signal peak amplitude versus the corresponding RH. We note that the signal strength varies with RH, and for the range of RH values corresponding to the test period, it is well above the shot-noise or the chosen threshold used in the spectrum rejection algorithm.

Aside from the functionality as a laser anemometer, as verified in Fig. 2, the SL-CDL can also be used to investigate other meteorologically relevant parameters. It can, for example, be configured to monitor particulate concentration in the atmosphere through further analysis of the amplitude profiles of the Doppler spectra (or even with chemical specificity if it is set up as a differential absorption lidar). The data in Fig. 3, fitted to $S = S_0(1 - \mathrm{RH}/100)^{-g}$ [15,16], $S_0 = 1.06$ and $g = 0.22$, shows that the SL-CDL may provide a coarse indication of the typical RH dependence of the aerosol backscatter coefficient (proportional to the signal). This is in agreement with previous studies which showed that, as humidity increases, tropospheric particles containing water-soluble (hygroscopic) material increase in size and thus in scattering cross-section [15,16].

In summary, we have demonstrated the state-of-the-art performance of an all-SL CDL for remote wind measurements in a field test. Our results experimentally confirmed that our SL-CDL can achieve a performance comparable to that of commercial lidars as manifested by the high correlation seen from the lidar-versus-sonic mean speed comparison. We have also found that the current portable SL-CDL can continuously operate with high data availability even under periodically changing outdoor conditions, both as a wind speed sensor and as an aerosol backscatter strength sensor. We believe that our proposed all-SL solution has a strong potential for realizing low-cost, mass-producible CDL sensors for various industrial applications.

We acknowledge the support of Windar Photonics A/S.

References

1. T. Fujii and T. Fukuchi, eds., *Laser Remote Sensing* (CRC Press, 2005).
2. S. Rahm, Opt. Lett. **26**, 319 (2001).
3. J. Mann, J.-P. Cariou, M. S. Courtney, R. Parmentier, T. Mikkelsen, R. Wagner, P. Lindelöw, M. Sjöholm, and K. Enevoldsen, Meteor. Z. **18**, 135 (2009).
4. R. Krishnamurthy, A. Choukulkar, R. Calhoun, J. Fine, A. Oliver, and K. S. Barr, Wind Energy doi:10.1002/we.539 (2012).
5. R. Wagner, M. Courtney, J. Gottschall, and P. Lindelöw-Marsden, Wind Energy **14**, 993 (2011).
6. M. J. Kavaya, S. W. Henderson, J. R. Magee, C. P. Hale, and R. Milton Huffaker, Opt. Lett. **14**, 776 (1989).
7. M. Harris, R. Young, F. Köpp, A. Dolfi, and J. Cariou, Aerospace Sci. Technol. **6**, 325 (2002).
8. C. Pedersen and R. S. Hansen, "Coherent lidar system based on a semiconductor laser and amplifier," U. S. patent application US 2010/0277714 A1 (November 4, 2010).
9. R. S. Hansen and C. Pedersen, Opt. Express **16**, 18288 (2008).
10. C. J. Karlsson, F. Å. A. Olsson, D. Letalick, and M. Harris, Appl. Opt. **39**, 3716 (2000).
11. P. J. Rodrigo and C. Pedersen, Opt. Express **18**, 5320 (2010).
12. M. Sjöholm, T. Mikkelsen, J. Mann, K. Enevoldsen, and M. Courtney, IOP Conf. Ser. Earth Environ. Sci. **1**, 012051 (2008).
13. D. A. Smith, M. Harris, A. S. Coffey, T. Mikkelsen, H. E. Jørgensen, J. Mann, and R. Danielian, Wind Energy **9**, 87 (2006).
14. P. Lindelöw-Marsden, www.upwind.eu/media/585/D6.1.3.pdf.
15. J. W. Fitzgerald, Appl. Opt. **23**, 411 (1984).
16. J-.S. Im, V. K. Saxena, and B. N. Wenny, J. Geophys. Res. **106**, 20213 (2001).